Can otolith microstructure and elemental fingerprints elucidate the early life history stages of the gadoid southern blue whiting (*Micromesistius australis australis*)?

Thomas A. J. Busbridge[a,b,c,*]
C. Tara Marshall[b]
Alexander I. Arkhipkin[c]
Zhanna Shcherbich[c]
Andy L. Marriott[d]
Paul Brickle[a,b]

[a]South Atlantic Environmental Research Institute, Stanley, FIQQ 1ZZ, Falkland Islands
[b]School of Biological Sciences, Zoology Building, University of Aberdeen, Aberdeen, AB24 2TZ, Scotland
[c]Falkland Islands Fisheries Department, Stanley, FIQQ 1ZZ, Falkland Islands
[d]Centre for Environmental Geochemistry, British Geological Survey, Nottingham, NG12 5GG, United Kingdom
*Corresponding author: tbusbridge@saeri.ac.fk

Keywords: *Micromesistius australis australis* – southern blue whiting – otolith microstructure – otolith microchemistry – early life history

Abstract

Southern blue whiting (*Micromesistius australis australis*) was one of the largest fisheries in the Southwest Atlantic with the peak in total annual catches attaining 258.000 tonnes. Intense exploitation over the past 30 years critically decreased its abundance and forced the implementation of a suite of conservation measures to save and rebuild the stocks. Recently improved recruitment levels require more information on the early life history stages of this fish. Using complimentary investigations into otolith microstructure and trace elemental composition by LA-ICPMS, larval, metamorphic and post-metamorphic periods of the early ontogeny were studied. The timing and completion of metamorphosis were estimated at 30.5 ± 0.3 and 60.7 ± 1.8 days after the first increment formation respectively. The timing of a newly defined 'juvenile transition-mark' (corresponding to the transition from the epipelagic larval habitat to a deeper juvenile habitat was estimated to form at age of 76.5 ± 2.0 days.

The movement of juveniles into deeper waters post-metamorphosis were further confirmed by significant shifts in the element:^{42}Ca ratios (for elements ^{24}Mg, ^{55}Mn, ^{88}Sr and ^{138}Ba). Elemental 'fingerprints' for each of the three otolith zones were further found to be distinct through high classification accuracies of the random Forest model (81.1 ± 0.1%). Holistic approach investigating both otolith microstructure and elemental composition provides further evidence that ontogeny could be a confounding factor in natal (geographic) origin studies if (1) otolith 'core' samples are taken from different ontogenetic otolith zones and (2) if elements predominantly controlled by physiology are included in the respective classification analyses.

1. Introduction

The southern blue whiting, *Micromesistius australis* (Norman, 1937), is a mesopelagic schooling fish that occupies waters around New Zealand and the tip of South America (Patagonia). The Patagonian sub-species *Micromesistius australis australis* once contributed to the largest fishery in the South Atlantic. However, following decades of exploitation and concerns over fluctuating landings the spawning stock biomass of *M. a. australis* is currently considered to be critically low (Laptikhovsky et al., 2013). The fishery has mainly targeted spawning aggregations of *M. a. australis* to the south-southwest of the Falkland Islands where spawning occurs between August – October (Macchi et al., 2005; Macchi and Pajaro, 1999; Pajaro and Macchi, 2001). Both egg and newly-hatched larval stages have previously been described for *M. a. australis* (Laptikhovsky and Brickle, 2009; Weiss, 1974), as well as embryogenesis (Laptikhovsky and Brickle, 2009). However, very little is known about subsequent stages of early ontogeny including the timing of metamorphosis and the juvenile stage.

Metamorphosis occurs when the larvae undergoes dramatic morphological and physiological changes during its development into a juvenile fish (Christensen and Korsgaard, 1999; Sæle et al., 2004). For many mesopelagic and benthic species the end of metamorphosis is marked by the transition from the pelagic larval habitat to the juvenile habitat in deeper waters, or settlement to demersal or benthic habitats (Biagi et al., 1998). Similar changes were previously observed in North Sea plaice (*Pleuronectes platessa*) by hatching larvae in laboratory conditions and monitoring their development and behaviour (Modin et al., 1996; Morales-Nin et al., 2005). In many gadoids the process of metamorphosis results in significant change to the otolith microstructure through the formation of accessory growth centres (AGCs) (Morales-Nin, 2000; Morales-Nin et al., 2005). As growth increments form and expand from the AGCs, they ultimately amalgamate to form a visible 'prism' around the otolith core (Morales-Nin et al., 2005). Combined observations of larval development and otolith growth revealed that the formation of the first and last formed AGC are associated with initiation and completion of metamorphosis respectively (Modin et al., 1996; Morales-Nin et al., 2005). The change in habitat between the larval and juvenile stages is visible within the otolith microstructure by means of a check mark resulting from a change in diet related to the change in habitat (Brothers, Edward et al., 1982; Victor, 1982). Although *M. a. australis* does not undergo settlement to the benthic habitat, a 'settlement mark' has previously been reported in *M. a. australis* otoliths (Barrera-Oro and Tomo, 1988). This mark in *M. a. australis* possibly corresponds to the transition of an individual from the pelagic larval habitat to a deeper, juvenile habitat. The timing at which these features are formed can be estimated through the usage of daily growth increment counts observed within the otolith microstructure (Arai et al., 2000; Buratti and Santos, 2010).

Besides structural changes, the otolith microchemistry is also thought to change throughout the early stages of ontogeny (Martin and Thorrold, 2005). For example, Brophy et al. (2004)

determined a Mn-rich core in Atlantic herring (*Clupea harengus*) otoliths. Additionally, Arai et al. (2000) reported significant shifts in ^{88}Sr:^{42}Ca ratios coinciding with the initiation and completion of metamorphosis. Longmore et al. (2011) further observed significant differences in various element:^{42}Ca ratios between samples taken from parts of the otolith corresponding to different stages of ontogeny. Multi-elemental signatures, or elemental 'fingerprints', are frequently used to classify between geographical locations to infer the stock structure or to reconstruct migration patterns of fishes (Campana, 1999; Campana and Thorrold, 2001). These studies assume differential rates of elemental uptake into the otolith microstructure based on the physical or chemical properties of the contemporaneous ambient environmental conditions which vary between geographical regions (Campana and Thorrold, 2001; Elsdon et al., 2008). The elemental shifts found in relation to ontogeny could confound the interpretations of these geographical origin studies. Macdonald et al. (2008), for example, revealed increased classification accuracies in the natal origin of three geographically isolated groups of Australian smelt (*Retropinna semoni*) when excluding the ^{55}Mn-rich otolith core (corresponding to the first period of life). Therefore, further elucidating on the relationship between ontogeny and otolith microchemistry is still required.

Here, we aim to estimate the timing and duration of the early stages of ontogeny in *M. a. australis* using the otolith microstructure and to investigate if the elemental 'fingerprints' corresponding to these putative stages are (1) distinct and (2) consistent with interpretations of a transition to a new life history stage.

2. Materials and Methods

2.1 Sample collection

Juvenile *M. a. australis* were sampled within the Falkland Interim Conservation and Management Zone (FICZ) between January and November 2017 (Figure 1).

INSERT FIGURE 1

Samples from January and February were collected during research cruises conducted by the Falkland Islands Fisheries Department (FIFD) aboard *RV Castelo* (ZDLT1), whereas samples from March to November were collected by FIFD fisheries observers from commercial trawls. Research and commercial trawls were conducted using bottom trawl nets with respective mesh sizes of 90 mm (including a 10-15 mm cod end liner) and 110 mm (no liner). Trawl depth ranged between 69 – 275 m and 120 - 287 m for research and commercial trawls respectively. Samples from the research cruises were frozen on board and later processed in the laboratory at the FIFD. Samples from the commercial trawls were processed at sea. Total length (cm) and total weight (g) were recorded for all samples, and otoliths were removed and stored in 95% ethanol. All individuals were considered juveniles (FIFD maturity scale) as gonads were too small to be classified correctly, with length-frequency analyses used to ensure samples belonged to the same cohort before further processing.

2.2 Sample preparation and interpretation

In the laboratory otoliths were mounted on slides and ground down manually on both sides to reveal the nucleus and daily growth increments following methods by Arkhipkin and Shcherbich (2012). However, a modification was required as the processing time of larger otoliths became impractical. For these samples initial grinding was performed using silicon carbide paper at differing coarse grades, e.g. P180 followed by P320/400, to reduce the thickness of the sample before polishing with P600 and P2000. It also became increasingly difficult to reveal clear growth increments from the nucleus to the otolith margin in the larger otoliths. Too thick a section left the primordium unclear, too thin a section and the otolith margin became unreadable (as described in Arkhipkin and Shcherbich (2012)). As a precautionary approach, counts within the primordium of larger otoliths were extrapolated. If

a preparation was uninterpretable, the second otolith was processed. In cases where interpretation of growth increments along a single radius was impossible, prominent growth increments or microstructural features were used to change the reading orientation (Morales-Nin and Aldebert, 1997) (Figure 2). Otoliths were initially read at 200x magnification (Olympus BX51) using transmitted light, but this was increased to 400x magnification towards the margin of larger otoliths where increments became narrower.

2.3 Timing of early life history stages

Initial increment counts were conducted from the nucleus (N) to the margin for all samples (Figure 2). The nucleus was hereby defined as the area of the otolith contained within the first discontinuous unit (Dunkelberger et al., 1980).

INSERT FIGURE 2

These 'total increment counts' were plotted against date of capture to confirm daily formation of the growth increments. Total increment counts were performed twice by Reader A (TB) and a subsample of 5 otoliths were read by Reader B (AA) to confirm reading precision. The otolith microstructure further revealed a number of features including a 'prism' shape with accessory growth centres (AGCs), and one or two distinct hyaline growth zones (the latter only visible in samples caught after July 2017). Increment counts were conducted up to the first formed AGC (AGC1), the last formed AGC (AGC2) and the first hyaline zone (HZ1) to estimate the age at which these features were formed. Three zones within the otolith sections were finally defined by these features according to their corresponding early life history stage: (A) larval (pre-metamorphosis) (N–AGC1), (B) metamorphosis (AGC1-AGC2) and (C) juvenile (AGC2-margin) (Figure 3).

2.4 Trace elemental analyses

147 A subsample of otoliths was further used to investigate the elemental composition of the
148 otolith throughout the early life history stages of *M. a. australis* by means of laser-ablation
149 inductively coupled plasma mass-spectrometry (LA-ICP-MS) at the British Geological
150 Survey, Keyworth, Nottingham, UK. Samples were re-mounted onto slides (dimensions 40 x
151 28 mm), decontaminated using 1%HNO_3/0.5%HCl solution and subsequently rinsed with
152 Milli-Q before placement into the chamber of the laser ablation system (NewWave UP-193).
153 Reference glasses NIST-610 and NIST-612 were used as external standards. To account for
154 mechanical drift, reference materials were ablated before and after samples, and reference
155 material NIST-610 was further ablated between individuals. For each otolith a line of spots
156 (spot size 35 µm, distance between spots 50 µm, dwell time = 30 s, wash-out time = 30 s)
157 was analysed from the nucleus to the anterior margin (Figure 3).

158 *INSERT FIGURE 3*

159 Irradiance (GW/cm^2) and fluence (J/cm^2) were recorded for each run. Raw counts (cps) of
160 trace elements (^{138}Ba, ^{42}Ca, ^{7}Li, ^{55}Mg, ^{24}Mn, ^{23}Na, ^{88}Sr) within the ablated material were
161 determined by ICP-MS (Agilent 7500c). Raw counts were converted to element
162 concentrations using Igor Pro 6.34 (Wavemetrics) and extension package Iolite v 2.5.
163 Elements for which counts were within detection limits (two SE of the background signal)
164 were removed from further analyses. Increment number (days after first increment formation)
165 and life history stage were determined for each spot. If a spot covered multiple growth
166 increments, the mean increment number was used.

167 *2.5 Statistical analyses*

168 All statistical analyses were performed in R V.3.5.1 (R Core Team, 2018). Data exploration
169 was conducted according to methods by Zuur et al. (2010) as summarised below.

170 *2.5.1 Age validation*

Average percent error (APE) (equation 1) was determined between total counts by Reader 1 (Comparison 1), and between the subsample read by Reader 1 and Reader 2 (Comparison 2) to confirm reading accuracy using R package 'FSA' (Ogle et al., 2018).

$$APE = \frac{\sum_{j=1}^{n} APEj}{n} \qquad \text{where} \qquad APEj = 100 \times \frac{\sum_{i=1}^{R} \frac{(xij - \bar{x}j)}{\bar{x}j}}{R} \qquad (1)$$

where *APEj* is the average percent error for the *jth* fish, *xij* is the *i*th age estimate on the *j*th fish, $\bar{x}j$ is the mean age estimate for the *j*th fish, *R* is the number of times that each fish was aged, and *n* is the number of aged fish in the sample (Beamish and Fournier, 1981). Systematic differences in age readings were determined using methods by Evans and Hoenig (1998). Samples were removed from further analyses if readings 1 and 2 by Reader A differed by >10%. Total number of growth increments were plotted against date of capture to confirm daily formation of growth increments. The data were fitted with a linear regression model of which the regression slope (*m*) was compared to 1 (*m* = 1 suggests: 1 growth increment = 1 day in age) to validate interpretation of the number of growth increments as age (days).

2.5.2 Age vs Length

The relationship between total length and age was visualised using a scatterplot. By increasing model complexity and checking model residuals a Gaussian GAM (family = quasipoisson), was produced for which the residual variation was homogenous and normally distributed. The 'predict' function in the 'Deriv'-package (Clausen and Sokol, 2018) was finally used to estimate the length (±SE) at Age = 365 days (1 year).

2.5.3 Trace elemental analyses

Elemental concentrations of the elements ^{138}Ba, ^{55}Mg, ^{24}Mn, ^{23}Na, ^{88}Sr were expressed as a ratio to ^{42}Ca. Elements ratios were used as explanatory variables with 'Zone' being the

response variable. Outliers in element:^{42}Ca were investigated. A distinction was made between outliers that were considered singular and outliers that were part of a 'peak' in element:^{42}Ca concentrations along individual profiles. Outliers applying to the former were removed from further analyses. Collinearity was observed between ^{88}Sr and ^{23}Na (0.83), of which ^{23}Na was removed upon inspection of the variance inflation factor values (VIF ^{23}Na = 3.54, VIF ^{88}Sr = 3.52). To account for the 2-dimensionality estimates of AGC1, AGC2, and HZ1, spots occurring within two SE of their respective mean estimates were removed from further analyses. Visualisation of the data included initial smoothed (method = LOESS, span = 0.8) element:^{42}Ca profiles against age, followed by boxplots depicting element:^{42}Ca ratio distribution against zone. Non-parametric Kruskal-Wallis tests were performed to compare median element:^{42}Ca ratios between life history stages with Wilcoxon rank post-hoc tests where pertinent. A random forest model was finally used to investigate multivariate differences in elemental composition of the otolith microstructure for the different early life history stages. The random forest model is a classification method which uses a subset (training subset) of the data to build classification trees (Breiman, 2001). The remaining data (prediction subset) is subsequently used to determine the prediction ability of those trees by trying a set number of variables, or elements in this study, at each node of the trees. See (Mercier et al., 2011) for more details on this model. Analyses were performed using R package 'randomForest' (Liaw and Wiener, 2002). In this study, the training:prediction data set ratio was 70:30, the number of classification trees computed was 500 and the number of variables tried at each split was 4. This procedure was repeated 1000 times. Classification results were converted to percentages (%), ranked, and the 50th, 500th and 950th observations for each value reported. Finally, the order of element contribution to classification accuracy was determined through a stepwise procedure using the Gini index (Breiman, 2001).

3. Results

219 *3.1 Increment interpretation and age validation*

220 100 individuals (TL range: 6 – 21 cm) were sampled between January and November 2017.
221 Total length was shown to increase with age (Figure 4). GAM regression parameters for
222 *s(Age)* were found to be significant (*edf* = 4.43, F = 227.8, p = <0.001) and the deviance
223 explained by the model was 92.9%. A reduction in growth rate (not calculated here) is visible
224 between 175-275 days, which corresponded to the austral winter period. Finally, TL at age 1
225 year (365 days) was estimated at 20.31 ± 0.48 cm.

226 *INSERT FIGURE 4*

227 GI counts were conducted using the methodology described in Section 2.2 (Figure 2). For 19
228 (22%) individuals the first otolith preparation was unreadable resulting in the second otolith
229 being utilised. APE for readings by Reader 1 (Comparison 1), and for the subsample read by
230 Reader 1 and Reader 2 (Comparison 2) were 1.7 and 1.1% respectively. No systematic
231 differences were further determined between readings (p = 0.40, p = 0.17 for Comparisons 1
232 and 2 respectively). Total increment counts ranged between 87-384 and increased with date
233 of capture (Figure 5).

234 *INSERT FIGURE 5*

235 The slope of the fitted linear model (m = 0.96) was compared against 1 (where 1 GI = 1 day)
236 and was found not to be significantly different (t-ratio = 0.571, p = 0.5693). Hereafter,
237 number of GIs was therefore interpreted as number of days. The linear model was further
238 used to estimate a mean date of first increment formation for the 2016-cohort as 03-11-2016.

239 *3.2 Timing of early life history stages*

240 Counts from the nucleus (N) to the first accessory growth centre (AGC1) revealed that the
241 initiation of metamorphosis occurred 26-34 days after first increment formation (mean 30.5 ±

0.3). In the larger otoliths for which reading between N - AGC1 was impossible, we therefore extrapolated this count at 31 increments. Counts further revealed that AGC2 formed 48-75 days after first increment formation (mean 60.7 ± 1.8). The average duration of metamorphosis was calculated by subtracting the mean number of increments at AGC2 from the mean number of increments for AGC1 (60.7 – 30.5) equating to 30.2 days. The next formed structural feature was the check mark. Counts indicated that the mark formed 60-91 days after first increment formation (mean 76.5 ± 2.0 inc.). These results suggest that the movement of juvenile *M. a. australis* into deeper waters occurs roughly 15.8 days after metamorphosis is completed (i.e. 76.5 – 60.7 days). The results further confirmed that this check mark formed during austral summer and should therefore not be interpreted as a winter annulus. The true winter annulus became visible in otoliths collected after July 2017 (austral winter).

3.3 Trace elemental analyses

15 Otoliths were successfully ablated and analysed from the core to the margin using LA-ICP-MS. Varying trends in element:^{42}Ca ratios were observed for the four elements ^{24}Mg, ^{55}Mn, ^{88}Sr and ^{138}Ba (Figure 6) and comparisons between ontogenetic zones revealed significant differences in element:^{42}Ca ratios for all elements (Table1).

INSERT FIGURE 6

^{24}Mg:^{42}Ca ratios ranged between $5.01e^{-5}$ – $2.57e^{-4}$ µmol·mol^{-1} across the three otolith zones. ^{24}Mg:^{42}Ca ratios were found to be significantly lower during metamorphosis compared to the larval (pre-metamorphosis) and juvenile otolith zones (p = 0.01 and $p = 1.90e^{-3}$ respectively). The opposite trend was observed for ^{55}Mn:^{42}Ca ratios which ranged between $7.94e^{-08}$ – $1.42e^{-05}$ µmol·mol^{-1}. Here, the onset of metamorphosis resulted in a significant increase in the ^{55}Mn:^{42}Ca ratios ($p = 6.30e^{-11}$). This decreased slightly after metamorphosis, but remained

significantly higher compared to the larval (pre-metamorphosis) zone ($p = 1.78e^{-03}$). ^{88}Sr:^{42}Ca ratios ranged between $1.97e^{-3}$ – $1.1e^{-2}$ mmol·mol^{-1} and were found to be significantly higher during the larval (pre-metamorphosis) phase compared to the metamorphosis and juvenile phases ($p = 7.20e^{-4}$ and $p = 8.10e^{-4}$ respectively). No statistical differences were found in ^{88}Sr:^{42}Ca ratios between the metamorphosis and juvenile otolith zones. ^{138}Ba:^{42}Ca ranged between $1.60e^{-06}$ – $1.92e^{-08}$ µmol·mol^{-1}. Unlike the other three elements included in this study, no shift was observed in ^{138}Ba:^{42}Ca ratios at the onset of metamorphosis. ^{138}Ba:^{42}Ca ratios were shown to remain stable throughout the entire larval period (including metamorphosis). However, ^{138}Ba:^{42}Ca ratios were found to be significantly higher in the juvenile zone compared to the larval (pre-metamorphosis) and metamorphosis zone ($p = 0.91e^{-3}$ and $p = 0.10e^{-3}$ respectively) possibly indicating a movement into deeper waters.

INSERT TABLE 1

Next, the single element:^{42}Ca data were combined and analysed using a multivariate random forest model to determine whether elemental fingerprints could be distinguished between different ontogenetic zones of the otolith. The model was iterated 1000 times and model classification accuracies ranged between 62.2 – 92.2 % (mean 81.1 ± 0.1 %). To further identify where correct and misclassification was occurring the results for the three zones were separated (Figure 7). Correct classification is indicated by filled squares (Figure 7). Distinct elemental fingerprints were determined for two out of three otolith zones (B and C). For zone A correct classification of spots ranged between 6.25 – 84.62 % (mean 52.3 ± 0.4 %). Spots from zone (A) had the highest misclassification rates at 37.0 ± 0.4 % and 10.7 ± 0.3 % for zones B and C respectively. This indicates the highest similarity in composition of the larval (pre-metamorphosis) zone elemental fingerprint with the metamorphosis zone fingerprint. Spots from the metamorphosis zone revealed the highest classification accuracy in this study at 74.4 – 100 % (mean 91.2 ± 0.1%). Misclassification of spots from zone B for zone A and

C was relatively low at 6.0 ± 0.1 and 2.8 ± 0.1 % respectively. This suggests that the shifts found in single element:^{42}Ca ratios during metamorphosis all contribute to create a distinct elemental fingerprint for this otolith zone. Classification accuracies for spots from the juvenile zone (C) ranged between 50.0 – 100 % (mean 77.9 ± 0.3 %). Classification error of spots from zone C was relatively low at 7.3 ± 0.2 and 14.8 ± 0.2 % for zones A and B respectively. The order of contribution to correct classification for the four elements was further determined as ^{55}Mn, ^{88}Sr, ^{24}Mg and finally ^{138}Ba.

INSERT FIGURE 7

4. Discussion

4.1 Age validation

A linear relationship was determined between date of capture and number of GIs within the otoliths of juvenile *M. a. australis.* This relationship validated the daily formation of the observed increments and revealed the mean date of first increment formation as 03-11-2016. The interpretation of, and age at, first increment formation in *M. a. australis* is currently unknown. In the European hake, *Merluccius merluccius,* age at first increment formation was determined at 8 days (Morales-Nin et al., 2005), corresponding to first exogenous feeding. Using this as a proxy for *M. a. australis* combined with a known embryogenic development time of up to ~8 days (Laptikhovsky and Brickle, 2009), reveals a mean spawning date of 18-10-2016. This falls within the estimated spawning period (Sep-Oct) observed for *M. a. australis* (Schubnikov *et al*. (1969) in (Barrera-Oro and Tomo, 1988; Pajaro and Macchi, 2001), further supporting our validation. TL was shown to increase throughout the first year of life, with a reduction in growth rate observed during the austral winter months (roughly between 175-275 days in age). Our GAM-predicted TL at age 1 year (365 days) of 20.31 cm was similar to the range (19.75 – 24.86 cm TL) reported in previous age and growth papers

(Zukowski & Liwoch (1977) in Barrera-Oro and Tomo (1988); Cassia, 2000). However, this study is the first to present validated age estimates for *M. a. australis*.

4.2 Timing of early life history events

The validated daily growth increments were further used to elucidate the timing and duration of early ontogenetic stages in *M. a. australis*. The order of formation of these microstructural features correspond to the order of the early life history events. Victor (1982) demonstrated through combined field observations and observations on the otolith microstructure that settlement in the wrasse *Halicoeres bivittatus* occurs before metamorphosis. In this study however, the otolith microstructure revealed that accessory growth centres formed before the check mark. From this we determined that metamorphosis occurred before the movement of juvenile *M. a. australis* into deeper waters. The initiation and completion of metamorphosis was estimated to occur 30.5 (± 0.3) and 60.7 (± 1.8) days respectively after first increment formation. Similar timings have been reported for the completion of metamorphosis in two separate Argentine hake (*Merluccius hubbsi*) populations at 64.1 - 66.7 days (Buratti and Santos, 2010), and for European hake *(Merluccius merluccius*) at 64 days after first increment formation (Morales-Nin et al., 2005). The check mark (HZ1) was further estimated to form 76.5 (± 2.0) days after first increment formation. Buratti and Santos (2010) estimated that in *M. hubbsi* the transition from pelagic to demersal habitat was completed ~80 days after first increment formation. These results suggest that the check mark in *M. a. australis* otoliths could therefore indicate the timing of movement to deeper waters in juvenile *M. a. australis*. Additionally, Barrera-Oro and Tomo (1988) were the first to suggest that the first check mark observed in *M. a. australis* otoliths was a settlement mark and proposed that this mark corresponded to a shift in habitat (and subsequently diet) rather than a period of reduced growth expected during the winter. Our results support this by showing that the check mark is formed 1) in austral summer and 2) shortly before the first juveniles appear as bycatch in the

bottom-trawl fishery. However, the term settlement mark is confusing for *M. a. australis* as this species does not undergo settlement. The term 'juvenile transition-mark' (JT-mark) is therefore proposed to describe the movement of juveniles from the pelagic larval habitat to the deeper, juvenile pelagic habitat. The second check mark was only observed in otoliths of older juveniles caught after the austral winter period which coincided with an observed reduction in growth. Using the otolith microstructure to infer the timing of shifts between early stages of ontogeny in *M. a. australis* could further be improved through tank-rearing experiments, where the formation of microstructural features can directly be linked to observed changes in behaviour and morphology (Modin et al., 1996).

4.3 Ontogenetic shifts in single element:^{42}Ca ratios

Mean element:^{42}Ca ratios reported in this study were similar to those previously reported for *M. a. australis* by Arkhipkin et al. (2009) and Niklitschek et al. (2010), except for ^{88}Sr (Table 2). Variation in these ratios is likely due to the sampling method used combined with the otolith area (and thus life history stage) studied (Table 2).

INSERT TABLE 2

Significant differences in element:^{42}Ca ratios between otolith zones were found for all elements studied. A significant reduction in ^{24}Mg:^{42}Ca ratios was observed during the metamorphosis period. ^{24}Mg incorporation into the otolith has been shown to be independent of temperature and salinity (Martin and Thorrold, 2005), indicating that ^{24}Mg is not a useful element to infer changes in habitat during early ontogeny. However, ^{24}Mg has been suggested to be under physiological control (Woodcock et al., 2012), with incorporation rates being negatively correlated with otolith precipitation rates and somatic growth (Martin and Thorrold, 2005). Our results, coupled with observations of increased daily increment width (a

363 proxy for otolith precipitation rates) in *M. a. australis* otoliths during metamorphosis, support
364 this.

365 The initiation of metamorphosis was shown to result in a significant increase in ^{55}Mn:^{42}Ca
366 ratios in the juvenile *M. a. australis* otoliths. Similar findings have been reported for juvenile
367 river herring (Alewife *Alosa pseudoharengus*) and blueback herring (*Alosa aestivalis*)
368 otoliths (Turner and Limburg, 2015). This increase was further positively correlated with
369 daily increment width (Turner and Limburg, 2015). Daily increments comprise of two units:
370 (1) a protein-rich layer and (2) a discontinuous, (typically) aragonite crystal layer (Morales-
371 Nin, 2000; Pannella, 1971). Areas of high precipitation rates are characterised by a relative
372 increase of protein-rich layer compared to the aragonite crystal layer (Morales-Nin, 2000),
373 and Izzo et al. (2016) revealed that a relatively large proportion of ^{55}Mn (up to 55.96%) is
374 incorporated into the protein-rich layer of the otolith (compared to 0.04 and 2.24 % for ^{88}Sr
375 and ^{138}Ba respectively). This was supported by Thomas et al. (2019) who suggested that ^{55}Mn
376 (II) ions are co-factors for the kinase *FAM20C* which regulates the biomineralisation of
377 otolith proteins. The increase in otolith-precipitation rates during metamorphosis could
378 therefore explain the shift in ^{55}Mn:^{42}Ca ratios.

379 ^{88}Sr:^{42}Ca ratios were shown to decrease throughout the early stages of ontogeny. Similar
380 findings have been reported for *Solea solea* (Pontual et al., 2003) and various *Anguilla sp.*
381 (Arai et al., 2000, 1999a, 1999b, 1999c, 1997). Incorporation rates of ^{88}Sr into the otolith
382 matrix has been widely studied, and are generally negatively correlated with ambient water
383 temperature (see Campana (1999)). The observed decrease in ^{88}Sr:^{42}Ca ratios within the
384 otoliths of juvenile *M. a. australis* therefore implies an increase in ambient water
385 temperature. Arkhipkin et al. (2004) observed a general warming trend within the first 100-
386 150m of the water column around the Falkland Islands during the austral summer months,
387 which could explain the decrease in ^{88}Sr:^{42}Ca ratios found in this study.

388 ^{138}Ba:^{42}Ca ratios have been shown to be positively correlated with dissolved organic matter,
389 which generally increases with depth (Ashford et al., 2005). No shift in ^{138}Ba:^{42}Ca ratios was
390 observed during metamorphosis in this study. However, an increase was observed for the
391 juvenile phase. This suggests the movement of *M. a. australis* into deeper, more productive
392 upwelling waters after metamorphosis has been completed. This shift could be the start of
393 their transition to the late juvenile/adult habitat depth range of 130-800 m (Niklitschek et al.,
394 2010).

395 *4.4 Classification between early life history stages using elemental 'fingerprints'*

396 This study revealed significant shifts in single element:^{42}Ca ratios between otolith material
397 laid down during different ontogenetic stages for all elements studied. Resulting classification
398 accuracies were consequently high for two out of three ontogenetic zones (91.2 – 77.9%
399 accuracy for zones B and C respectively). Misclassification of spots from zone A was high
400 (47.7 ± 0.3%) and was possibly due to the large variability found in the elemental signatures
401 in this zone, or by having the lowest number of spots available to train the random forest
402 model. However, a mean classification accuracy of 81.1 ± 0.01 % suggests that the random
403 forest model was an appropriate method for our classification analyses. The relative
404 simplicity in implementing the random forest model (i.e. no assumed relationship between
405 variables and raw input data) further advocates the use of this classification method for
406 otolith chemistry data. Classification accuracies can be improved by selecting for the optimal
407 number of elements, where the inclusion of more elements does not necessarily improve
408 classification (Mercier et al. (2011); however, see Marriott et al. (2016)). In this study, a high
409 classification accuracy was determined for spots taken from different ontogenetic zones, with
410 ^{55}Mn being the highest contributor to classification accuracy. It could therefore be argued that
411 when using elemental 'fingerprints' to investigate natal origin, for example, elements such as
412 ^{55}Mn should be excluded to avoid confounding ontogenetic signals. This is supported by

413 Macdonald et al. (2008) who revealed increased classification accuracies in the natal origin of
414 three geographically isolated groups of Australian smelt (*Retropinna semoni*) when excluding
415 the ^{55}Mn-rich primordium of the otolith.

416 This study revealed that changes to the otolith microstructure of gadoid otoliths can be
417 correlated with changes in microchemistry. We further showed that ontogenetic signals
418 complied with traditional interpretations of certain elements in otolith chemistry data. For
419 future studies element selection must therefore be carefully tailored to address the aims of the
420 study. Element affinity to either the protein- or aragonite layer should also be taken into
421 account when selecting for elements. A study comparing classification accuracies using
422 'protein-elements' vs 'aragonite-elements' could provide further insights into optimal
423 element selection in future otolith chemistry research.

424 **Acknowledgements**

425 The authors would like to thank Dr. Simon Chenery and the British Geological Survey group
426 for the LA-ICP-MS equipment training and data processing. We would further like to extend
427 our thanks to the Falkland Islands Government Fisheries Department and its scientific
428 fisheries observers for providing the materials used in this study. Our thanks also go to Dr.
429 Jessica Jones, Brendon Lee and the anonymous referees for their comments which helped
430 improve this manuscript. The authors would finally like to thank Fortuna Ltd. for enabling
431 this project through their generous funding.

432 **References**

433 Arai, T., Limbong, D., Otake, T., Tsukamoto, K., 1999a. Metamorphosis and inshore
434 migration of tropical eels Anguilla spp . in the Indo-Pacific. Mar. Ecol. Prog. Ser. 182,
435 283–293.

436 Arai, T., Otake, T., Jellyman, D.J., Tsukamoto, K., 1999b. Differences in the early life history

437 of the Australasian shortfinned eel Anguilla australis from Australia and New Zealand ,
438 as revealed by otolith microstructure and microchemistry. Mar. Biol. 135, 381–389.

439 Arai, T., Otake, T., Limbong, D., Tsukamoto, K., 1999c. Early life history and recruitment of
440 the tropical eel Anguilla bicolor pacifica , as revealed by otolith microstructure and
441 microchemistry. Mar. Biol. 133, 319–326.

442 Arai, T., Otake, T., Tsukamoto, K., 2000. Timing of metamorphosis and larval segregation of
443 the Atlantic eels Anguilla rostrata and A. anguilla, as revealed by otolith microstructure
444 and microchemistry. Mar. Biol. 137, 39–45. https://doi.org/10.1007/s002270000326

445 Arai, T., Otake, T., Tsukamoto, K., 1997. Drastic changes in otolith microstructure and
446 microchemistry accompanying the onset of metamorphosis in the Japanese eel Anguilla
447 japonica. Mar. Ecol. Prog. Ser. 161, 17–22.

448 Arkhipkin, A.I., Grzebielec, R., Sirota, A.M., Remeslo, A. V., Polishchuk, I.A., Middleton,
449 D.A.J., 2004. The influence of seasonal environmental changes on ontogenetic
450 migrations of the squid Loligo gahi on the Falkland shelf. Fish. Oceanogr. 13, 1–9.
451 https://doi.org/10.1046/j.1365-2419.2003.00269.x

452 Arkhipkin, A.I., Schuchert, P.C., Danyushevsky, L., 2009. Otolith chemistry reveals fine
453 population structure and close affinity to the Pacific and Atlantic oceanic spawning
454 grounds in the migratory southern blue whiting (Micromesistius australis australis). Fish.
455 Res. 96, 188–194. https://doi.org/10.1016/j.fishres.2008.11.002

456 Arkhipkin, A.I., Shcherbich, Z.N., 2012. Thirty years' progress in age determination of squid
457 using statoliths. J. Mar. Biol. Assoc. United Kingdom 92, 1389–1398.
458 https://doi.org/10.1017/S0025315411001585

459 Ashford, J.R., Jones, C.M., Hofmann, E., Everson, I., Moreno, C., Duhamel, G., Williams,

460 R., 2005. Can otolith elemental signatures record the capture site of Patagonian
461 toothfish (Dissostichus eleginoides) , a fully marine fish in the Southern Ocean? . Can.
462 J. Fish. Aquat. Sci. 62, 2832–2840. https://doi.org/10.1139/f05-191

463 Barrera-Oro, E.R., Tomo, A.P., 1988. New information on Age and Growth in Length of
464 Micromesistius australis, Norman 1937 (Pisces, Gadidae), in the South-West Atlantic.
465 Polar Biol. 8, 341–351.

466 Beamish, R.J., Fournier, D.A., 1981. A Method for Comparing the Precision of a Set of Age
467 Determinations. Can. J. Fish. Aquat. Sci. 38, 982–983. https://doi.org/10.1139/f81-132

468 Biagi, F., Gambaccini, S., Zazzetta, M., 1998. Settlement and recruitment in fishes: The role
469 of coastal areas. Ital. J. Zool. 65, 269–274. https://doi.org/10.1080/11250009809386831

470 Breiman, L., 2001. Random forests. Mach. Learn. 45, 5–32.
471 https://doi.org/10.1007/9781441993267_5

472 Brophy, D., Jeffries, T.E., Danilowicz, B.S., 2004. Elevated manganese concentrations at the
473 cores of clupeid otoliths: Possible environmental, physiological, or structural origins.
474 Mar. Biol. 144, 779–786. https://doi.org/10.1007/s00227-003-1240-3

475 Brothers, Edward, B., Prince, E.D., Lee, D.W., 1982. Age and growth of young-of-the-year
476 bluefin tuna , Thunnus thynnus , from otolith microstructure. Proc. Int. Work. Age
477 Determ. Ocean. Pelagic Fishes Tunas, Billfishes, Sharks, Vol. NOAA Tech. Rep. NMFS
478 8 49–59.

479 Buratti, C.C., Santos, B.A., 2010. Otolith microstructure and pelagic larval duration in two
480 stocks of the Argentine hake, Merluccius hubbsi. Fish. Res. 106, 2–7.
481 https://doi.org/10.1016/j.fishres.2010.05.007

482 Campana, S.E., 1999. Chemistry and composition of fish otoliths: pathways, mechanisms and

483 applications. Mar. Ecol. Prog. Ser. 188, 263–297.

484 Campana, S.E., Thorrold, S.R., 2001. Otoliths, increments, and elements: keys to a
485 comprehensive understanding of fish populations? Can. J. Fish. Aquat. Sci. 58, 30–38.

486 Cassia, M.C., 2000. Age and growth of the southern blue whiting Micromesistius australis in
487 the SW Atlantic. Sci. Mar. 64, 269–274. https://doi.org/10.3989/scimar.2000.64n3269

488 Christensen, M.N., Korsgaard, B., 1999. Protein metabolism, growth and pigmentation
489 patterns during metamorphosis of plaice (Pleuronectes platessa) larvae. J. Exp. Mar. Bio.
490 Ecol. 237, 225–241. https://doi.org/10.1016/S0022-0981(98)00215-9

491 Clausen, A., Sokol, S., 2018. Deriv: R-based Symbolic Differentiation. Deriv package
492 version 3.8.

493 Dunkelberger, D.G., Dean, J.M., Watabe, N., 1980. The Ultrastructure of the Otolithic
494 Membrane and Otolith in the Juvenile Mummichog , Fundulus heteroclitus 163, 367–
495 377.

496 Elsdon, T., Wells, B., Campana, S., Gillanders, B., Jones, C., Limburg, K., Secor, D.,
497 Thorrold, S., Walther, B., 2008. Otolith Chemistry To Describe Movements And Life-
498 History Parameters Of Fishes: Hypotheses, Assumptions, Limitations and Inferences.
499 Oceanogr. Mar. Biol. 46, 297–330. https://doi.org/10.1201/9781420065756.ch7

500 Evans, G.T., Hoenig, J.M., 1998. Testing and Viewing Symmetry in Contingency Tables ,
501 with Application to Readers of Fish Ages. Int. Biometric Soc. 54, 620–629.

502 Izzo, C., Doubleday, Z.A., Gillanders, B.M., 2016. Where do elements bind within the
503 otoliths of fish? Mar. Freshw. Res. 67, 1072–1076.

504 Laptikhovsky, V., Arkhipkin, A., Brickle, P., 2013. From small bycatch to main commercial
505 species: Explosion of stocks of rock cod Patagonotothen ramsayi (Regan) in the

506 Southwest Atlantic. Fish. Res. 147, 399–403.
507 https://doi.org/10.1016/j.fishres.2013.05.006

508 Laptikhovsky, V., Brickle, P., 2009. Aspects of embryonic development in two southwest
509 Atlantic gadiform fish: Tadpole codling, Salilota australis (Moridae), and southern blue
510 whiting, Micromesistius australis (Gadidae). Acta Ichthyol. Piscat. 39, 127–130.
511 https://doi.org/10.3750/AIP2009.39.2.07

512 Liaw, A., Wiener, M., 2002. Classification and Regression by randomForest. R News 18–22.
513 https://doi.org/10.1177/154405910408300516

514 Longmore, C., Trueman, C.N., Neat, F., O'Gorman, E.J., Milton, J.A., Mariani, S., 2011.
515 Otolith geochemistry indicates life-long spatial population structuring in a deep-sea fish,
516 Coryphaenoides rupestris. Mar. Ecol. Prog. Ser. 435, 209–224.
517 https://doi.org/10.3354/meps09197

518 Macchi, G.J., Pajaro, M., 1999. Reproductive habitat, biology and acoustic biomass estimates
519 of the southern blue whiting (Micromesistius australis) in the sea off southern Patagonia.
520 INIDEP Doc. Cient. 5, 67–79.

521 Macchi, G.J., Pájaro, M., Wöhler, O.C., Acevedo, M.J., Centurión, R.L., Urteaga, D.G.,
522 2005. Batch fecundity and spawning frequency of southern blue whiting
523 (Micromesistius australis) in the southwest Atlantic Ocean. New Zeal. J. Mar. Freshw.
524 Res. 39, 993–1000. https://doi.org/10.1080/00288330.2005.9517370

525 Macdonald, J.I., Shelley, J.M.G., Crook, D.A., 2008. A Method for Improving the Estimation
526 of Natal Chemical Signatures in Otoliths. Trans. Am. Fish. Soc. 137, 1674–1682.
527 https://doi.org/10.1577/t07-249.1

528 Marriott, A.L., McCarthy, I.D., Ramsay, A.L., Chenery, S.R.N., 2016. Discriminating

529 nursery grounds of juvenile plaice (Pleuronectes platessa) in the south-eastern Irish Sea
530 using otolith microchemistry. Mar. Ecol. Prog. Ser. 546, 183–195.
531 https://doi.org/10.3354/meps11664

532 Martin, G.B., Thorrold, S.R., 2005. Temperature and salinity effects on strontium
533 incorporation in otoliths of larval spot (Leiostomus xanthurus). Mar. Ecol. Prog. Ser.
534 293, 223–232. https://doi.org/10.1139/F03-143

535 Mercier, L., Darnaude, A.M., Bruguier, O., Vasconcelos, R.P., Cabral, H.N., Costa, M.J.,
536 Lara, M., Jones, D.L., Mouillot, D., 2011. Selecting statistical models and variable
537 combinations for optimal classification using otolith microchemistry. Ecol. Appl. 21,
538 1352–1364.

539 Modin, J., Fagerholm, B., Gunnarsson, B., Pihl, L., 1996. Changes in otolith microstructure
540 at metamorphosis of plaice, Pleuronectes platessa L. ICES J. Mar. Sci. 53, 745–748.

541 Morales-Nin, B., 2000. Review of the growth regulation processes of otolith daily increment
542 formation. Fish. Res. 46, 53–67. https://doi.org/10.1016/S0165-7836(00)00133-8

543 Morales-Nin, B., Aldebert, Y., 1997. Growth of juvenile Merluccius merluccius in the Gulf
544 of Lions (NW Mediterranean) based on otolith microstructure and length-frequency
545 analysis. Fish. Res. 30, 77–85.

546 Morales-Nin, B., Bjelland, R.M., Moksness, E., 2005. Otolith microstructure of a hatchery
547 reared European hake (Merluccius merluccius). Fish. Res. 74, 300–305.
548 https://doi.org/10.1016/j.fishres.2005.03.001

549 Niklitschek, E.J., Secor, D.H., Toledo, P., Lafon, A., George-Nascimento, M., 2010.
550 Segregation of SE Pacific and SW Atlantic southern blue whiting stocks: integrating
551 evidence from complementary otolith microchemistry and parasite assemblage

552 approaches. Environ. Biol. Fishes 89, 399–413. https://doi.org/10.1007/s10641-010-
553 9695-9

554 Norman, J.R., 1937. Coast Fishes XVI, 1–150.

555 Ogle, D., Wheeler, P., Dinno, A., 2018. FSA: Fisheries Stock Analysis. R package version
556 0.8.22.

557 Pajaro, M., Macchi, G.J., 2001. Spawning pattern, length at maturity, and fecundity of the
558 southern blue whiting (Micromesistius australis) in the south-west Atlantic Ocean. New
559 Zeal. J. Mar. Freshw. Res. 35, 375–385.
560 https://doi.org/10.1080/00288330.2001.9517008

561 Pannella, G., 1971. Fish otoliths: daily growth layers and periodical patterns. Science (80-.).
562 173, 1124–1127.

563 Pontual, H. De, Lagardère, F., Amara, R., Bohn, M., Ogor, A., 2003. Influence of ontogenetic
564 and environmental changes in the otolith microchemistry of juvenile sole (Solea solea).
565 J. Sea Res. 50, 199–210. https://doi.org/10.1016/S

566 Sæle, Ø., Solbakken, J.S., Watanabe, K., Hamre, K., Power, D., Pittman, K., 2004. Staging of
567 Atlantic halibut (Hippoglossus hippoglossus L.) from first feeding through
568 metamorphosis, including cranial ossification independent of eye migration.
569 Aquaculture 239, 445–465. https://doi.org/10.1016/j.aquaculture.2004.05.025

570 Thomas, O.R.B., Swearer, S.E., Kapp, E.A., Peng, P., Tonkin-hill, G.Q., Papenfuss, A.,
571 Roberts, A., Bernard, P., Roberts, B.R., 2019. The inner ear proteome of fish. Fed. Eur.
572 Biochem. Soc. 286, 66–81. https://doi.org/10.1111/febs.14715

573 Turner, S.M., Limburg, K.E., 2015. Does Daily Growth Affect the Rate of Manganese
574 Uptake in Juvenile River Herring Otoliths? Trans. Am. Fish. Soc. 144, 873–881.

https://doi.org/10.1080/00028487.2015.1059888

Victor, B.C., 1982. Daily otolith increments and recruitment in two coral-reef wrasses, Thalassoma bifasciatum and Halichoeres bivittatus. Mar. Biol. 71, 203–208. https://doi.org/10.1007/BF00394631

Weiss, G., 1974. Finding and description of larvae of Micromesistius australis in Patagonic waters of Argentina (Pisces, Gadidae). PHYSIS Secc. A. 33, 537–542.

Woodcock, S.H., Munro, A.R., Crook, D.A., Gillanders, B.M., 2012. Incorporation of magnesium into fish otoliths: Determining contribution from water and diet. Geochim. Cosmochim. Acta 94, 12–21. https://doi.org/10.1016/j.gca.2012.07.003

Zuur, A.F., Ieno, E.N., Elphick, C.S., 2010. A protocol for data exploration to avoid common statistical problems. Methods Ecol. Evol. 1, 3–14. https://doi.org/10.1111/j.2041-210x.2009.00001.x

Table

Table 1. Summary table for median element/Ca ratios per zone (All = all zones, A = larval, B = metamorphosis, C = juvenile) in *M. a. australis* otoliths. N = number of laser ablation spots available per zone. Summary statistics for elemental comparisons between all zones (Kruskal-Wallis rank sum test) and pairwise post-hoc (Wilcoxon rank sum test) comparisons between zones (A = zone A, B = zone B, and C = zone C) are also shown. MAD equals Median Absolute Deviation.

					Kruskal-Wallis comparisons			*Wilcoxon post-hoc comparisons*	
Element	Zone	N	Median	MAD	df	Chi^2	*p*	A	B
^{24}Mg	All	359	9.77e-05	4.02e-05	2	14.695	6.44e-04*		
	A	69	1.04e-04	4.51e-05					
	B	200	8.81e-05	3.39e-05				0.01*	
	C	90	1.06e-04	3.60e-05				0.76	1.90e-3*
^{55}Mn	All	359	5.89e-06	4.15e-06	2	38.72	3.91e-09*		
	A	69	3.04e-06	1.68e-06					
	B	200	6.91e-06	3.23e-06				6.30e-11*	
	C	90	5.00e-06	5.00e-06				1.78e-03*	0.05
^{88}Sr	All	359	4.65e-03	1.71e-03	2	9.2276	9.91e-03*		
	A	69	5.25e-03	1.20e-03					
	B	200	4.36e-03	1.52e-03				7.20e-04*	
	C	90	4.14e-03	1.47e-03				8.10e-04*	0.36
^{138}Ba	All	359	4.62e-06	2.13e-06	2	19.133	7.01e-05*		
	A	69	4.43e-06	1.51e-06					
	B	200	4.33e-06	2.11e-06				0.95	
	C	90	5.32e-06	1.82e-06				0.91e-03*	0.10e-03*

* indicates significance

Table 2. Mean element:^{42}Ca ratios determined in this study, Arkhipkin et al. (2009) and Niklitschek et al. (2010) for *M. a. australis* otoliths.

	Methodology	Sample region	^{24}Mg	^{55}Mn	^{88}Sr	^{138}Ba
This study	spot analyses	juvenile (< 4 months)	108	6	4730	5
Arkhipkin *et al.* (2009)	spot analyses (otolith core)	Juvenile (< 4 months)	18	2	1909	3
Niklitschek *et al.* (2010)	dissolved otolith fragments	juvenile (< 1 year)	300	18	2340	11

Figure

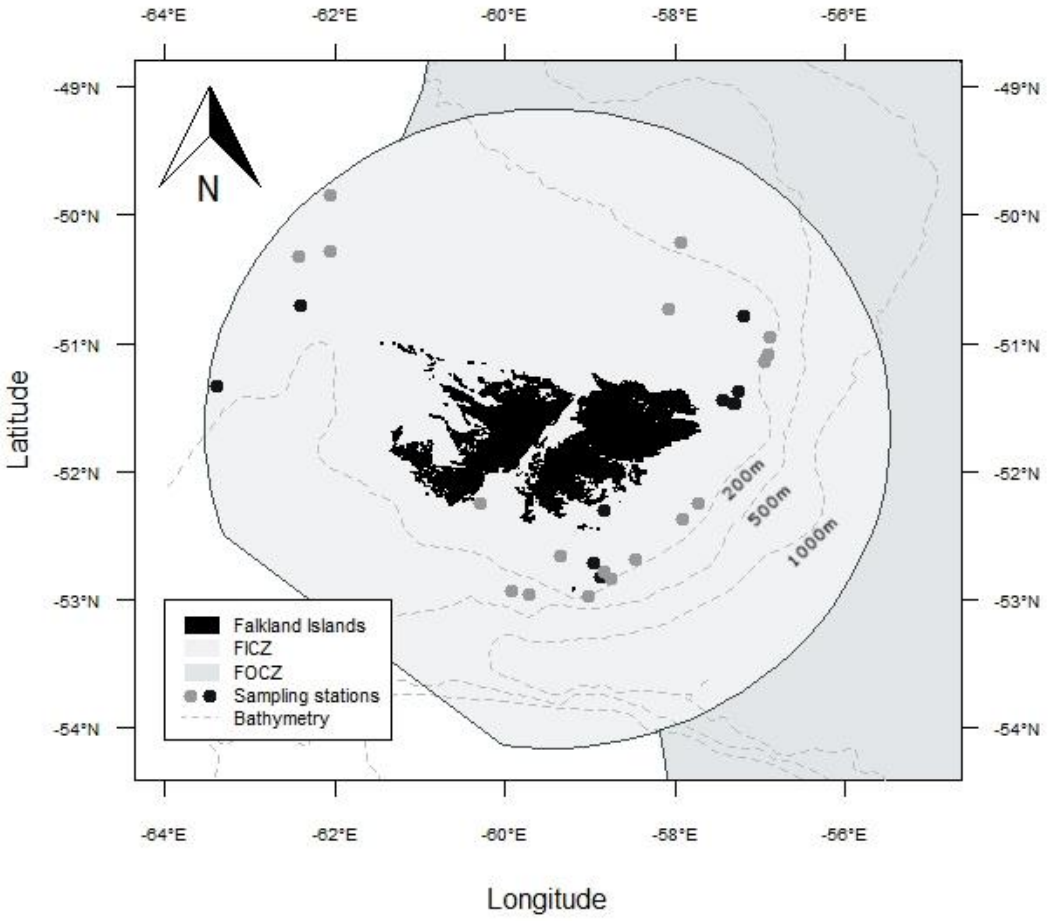

Figure 1. Map of sampling stations within the Falkland Interim Conservation and Management Zone (FICZ). Samples from all stations were used for age validation, and the dark grey stations indicate which samples were further subsampled for trace elemental analyses. FOCZ represents the Falklands Outer Conservation Zone.

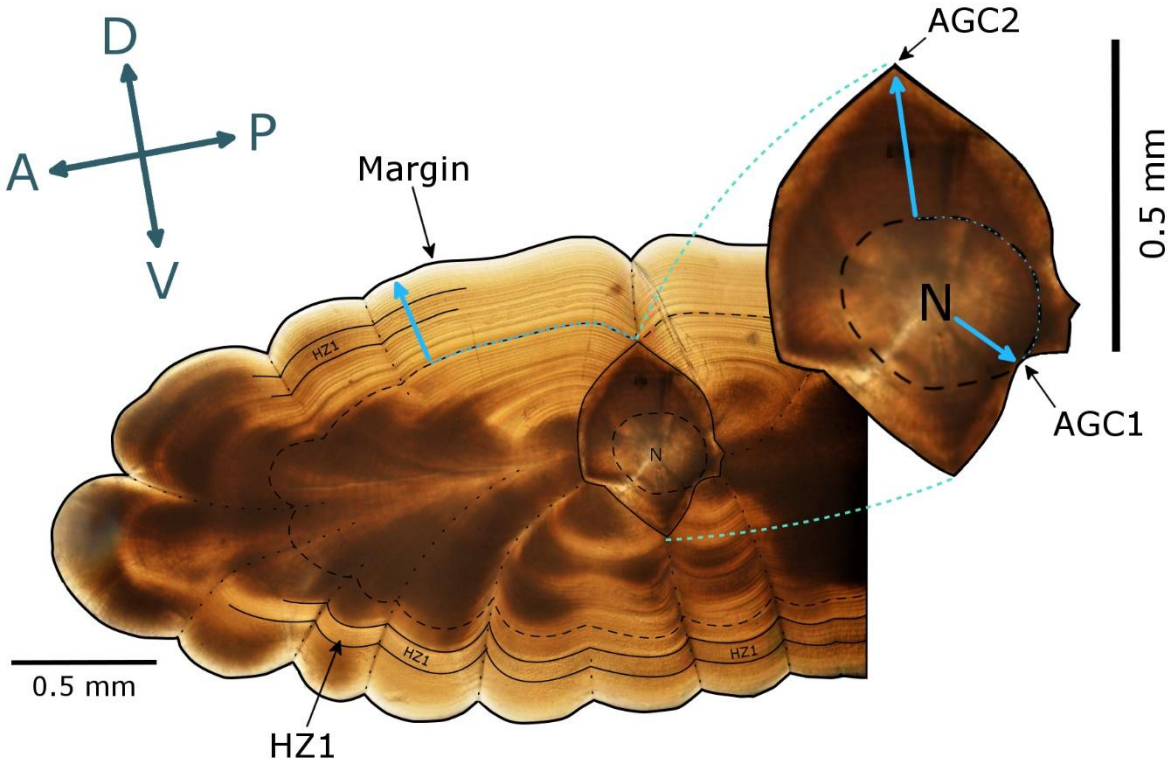

Figure 2. Juvenile *M. a. australis* (TL = 8 cm, 86 days) otolith section ground down to reveal the nucleus (N), prism shape (inset), accessory growth centres (i.e. AGC1, AGC2) and the first hyaline zone (HZ1). Blue arrows indicate direction of reading, blue dashed lines indicate change of reading orientation. Black dashed lines indicate shape of otolith at AGC1 and AGC2 respectively. Top left compass indicates anterior (A), posterior (P), dorsal (D) and ventral (V) orientation of otolith. Scale bars shown for otolith and inset respectively.

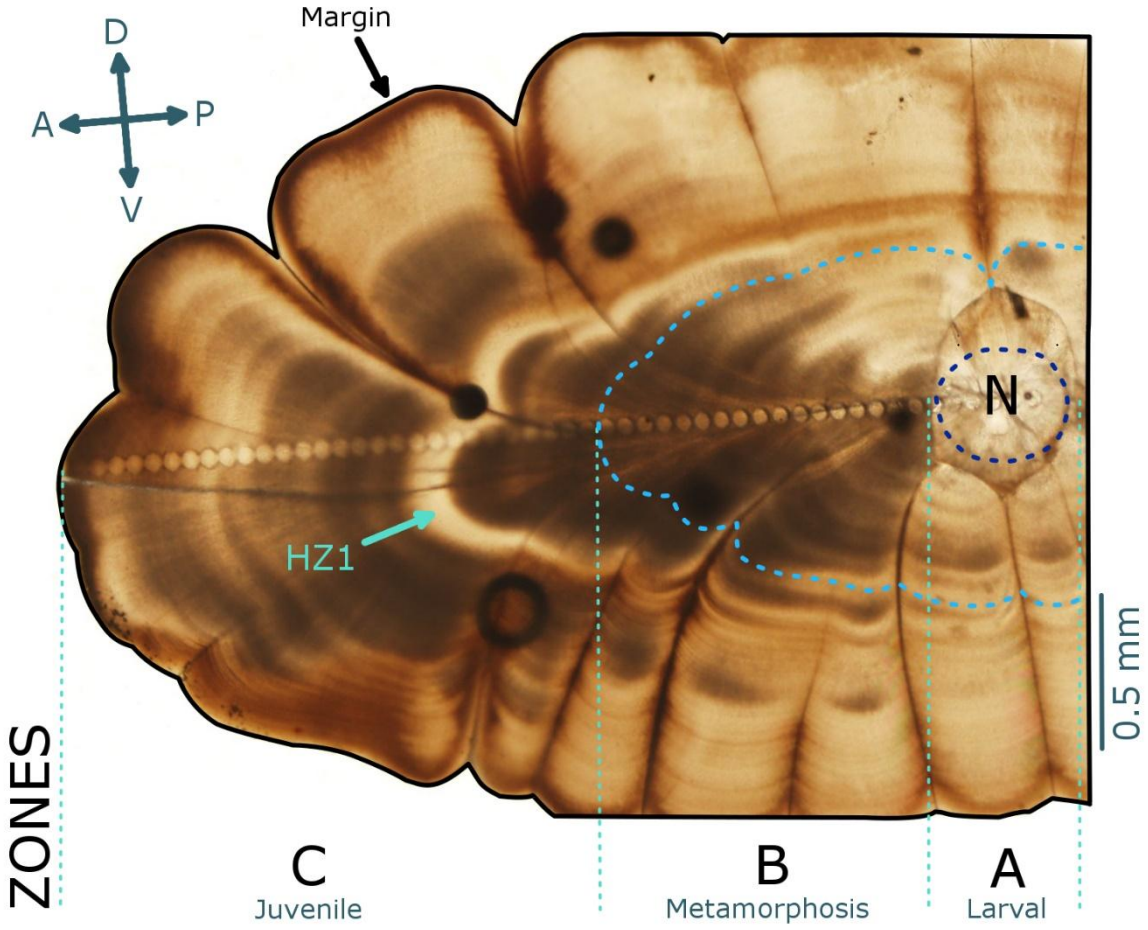

Figure 3. Juvenile *M. a. australis* (12 cm TL, 142 days) otolith section showing line of ablation spots analysed from the nucleus (N) to the margin, covering the first formed hyaline zone (HZ1). Larval and subsequent metamorphosis zones are outlined (dashed lines) to indicate significant change in otolith shape during metamorphosis.

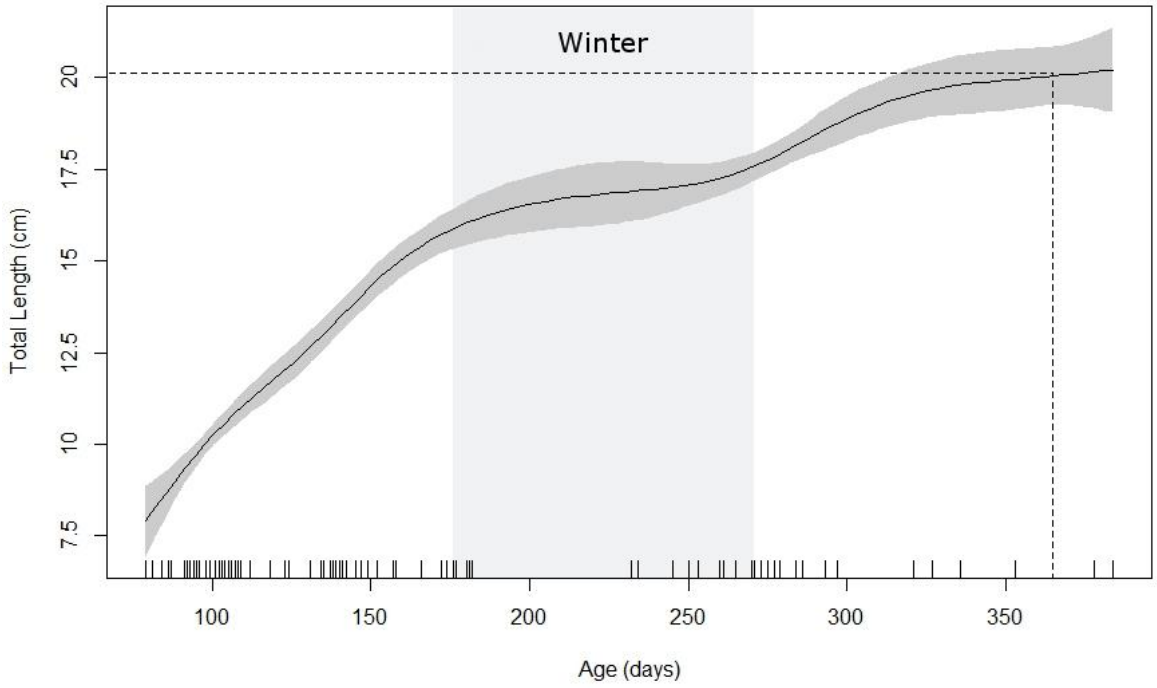

Figure 4. Relationship between total length (cm) and (smoothed) age (days) in juvenile *M. a. australis* of the 2016-cohort. 95% confidence intervals are depicted as shaded bands. Dashed lines indicate total length at 1 year of age. Rug depicts distribution of the data. Austral winter period is indicated by shaded area.

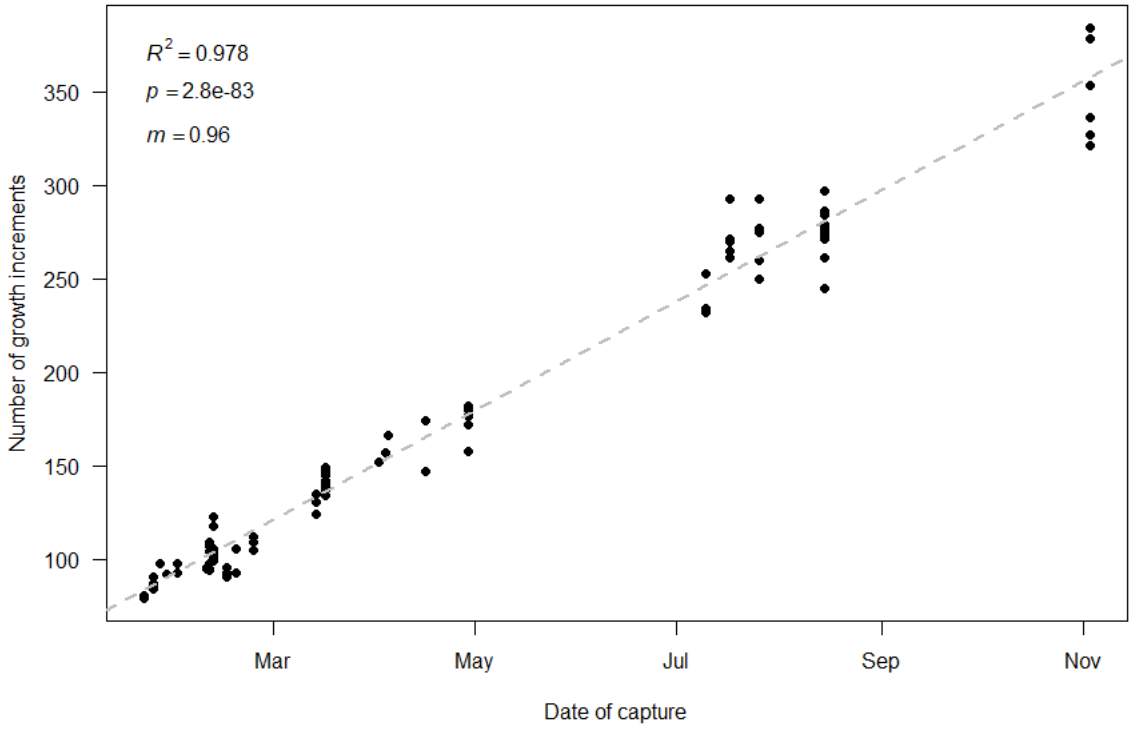

Figure 5. Number of growth increments within juvenile *M. a. australis* otoliths plotted against date of capture. Data was fitted with a (dashed) trend line for which the regression parameters R-squared, significance and slope are shown in figure.

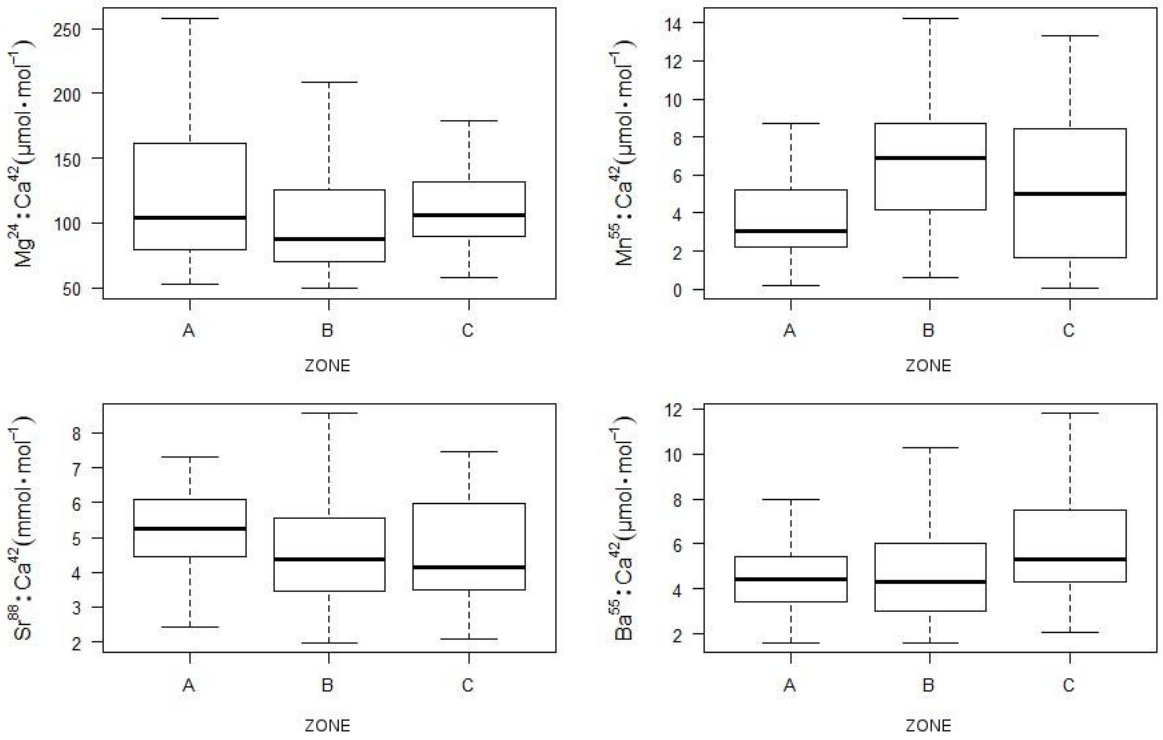

Figure 6. Boxplots depicting median element:^{42}Ca ratios found in different zones (A=larval (pre-metamorphosis), B=metamorphosis, C=juvenile) of *M. a. australis* otoliths. All observations are contained between the lower and upper whiskers (1st and 100th percentile respectively). The lower and upper quartiles represent the 25th and 75% percentile respectively.

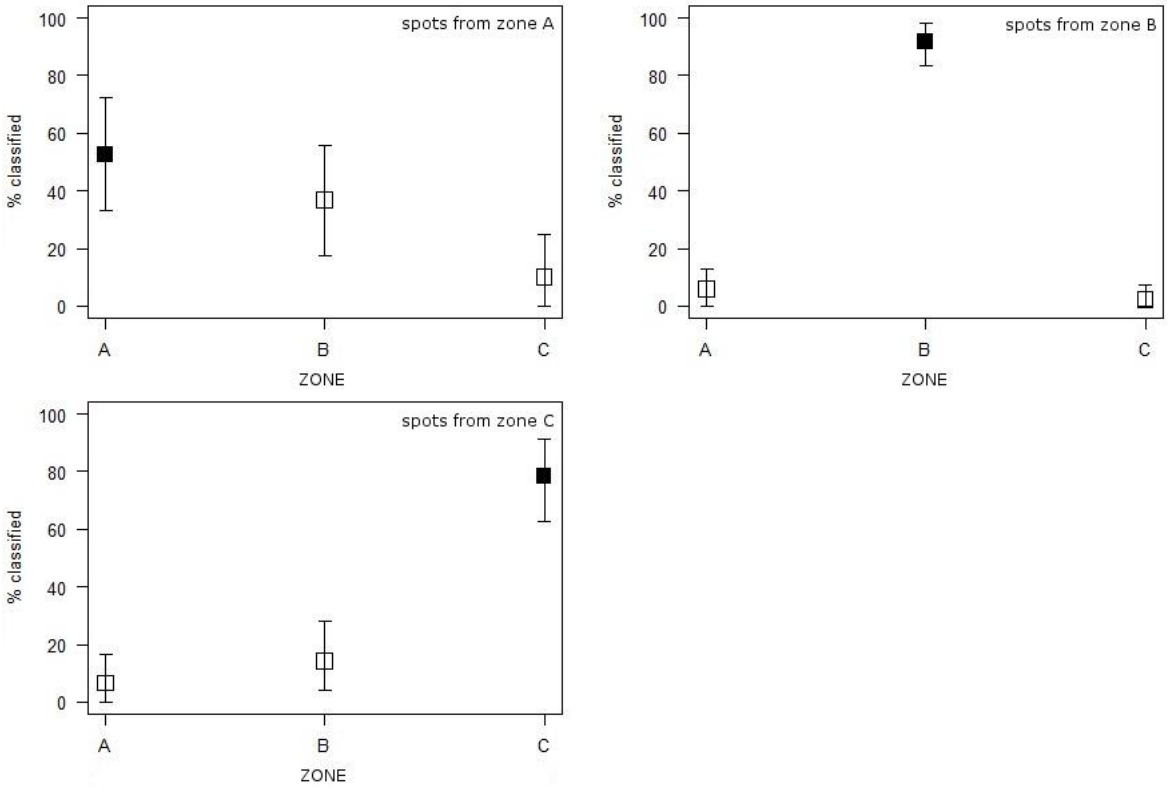

Figure 7. Percentage of spots assigned to each zone (x-axes: A = larval (pre-metamorphosis), B = metamorphosis, C = juvenile) in the random forest model. Model was repeated 1000 times and data points (squares) represent the median

(500th) observed values with top and lower error bars representing the 950th and 50th observed values respectively. Filled squares = correct classification, empty squares = classification error.